scientific reports

Check for updates

OPEN

Zone-inspired hydrogel constructs promote spatially controlled chondrogenesis for osteochondral regeneration

Ekin Çelik[1]✉, Cem Bayram[2] & Emir Baki Denkbaş[3,4]

Mimicking the structural and functional complexity of native articular cartilage remains a major challenge in osteochondral tissue engineering. In this study, we developed a multilayer hydrogel construct composed of methacrylated chondroitin sulfate (CSMA), gelatin methacryloyl (GelMA), polyethylene glycol dimethacrylate (PEGDMA), and nano-hydroxyapatite (nHA), engineered to replicate the biochemical and biomechanical gradients of the cartilage zones. Each hydrogel layer was systematically tailored to reflect the hydration, stiffness, porosity, and degradation profiles of the superficial, middle, and deep cartilage zones. Mechanical testing revealed a progressive increase in compressive modulus, while SEM imaging demonstrated tunable porosity across layers. PEGDMA incorporation enhanced structural integrity and reduced enzymatic degradation. In vitro chondrocyte encapsulation confirmed high cell viability and zone-specific gene expression, COL2A1 was elevated in GelMA-based middle layers, and COL10A1 was upregulated in nHA-enriched deep layers. Collagen type II immunofluorescence further supported sustained chondrogenic activity. Although whole-construct biological assessment was limited due to post-crosslinking homogenization, characterization of individual layers affirmed their zonal functionality. These findings establish a robust and reproducible platform for stratified hydrogel design and highlight its potential in advancing biomimetic strategies for osteochondral repair.

Keywords Zonal cartilage, GelMA, CSMA, Hydrogel engineering, Osteochondral regeneration, Chondrogenic differentiation

Articular cartilage damage, arising from trauma, aging, or degenerative disorders such as osteoarthritis, remains a major therapeutic challenge[1]. Owing to its avascular, aneural, and alymphatic structure, cartilage exhibits minimal intrinsic regenerative capacity[2,3]. Current treatment strategies primarily focus on managing symptoms, including pain relievers and intra-articular hyaluronic acid injections, which aim to slow disease progression in the early stages of degeneration[4]. However, in advanced cases, surgical interventions such as arthroplasty or mosaicplasty remain the only viable options for cartilage repair, despite their associated limitations and potential complications.

In recent years, tissue engineering has emerged as a promising alternative for cartilage regeneration[5–9]. Among the various biomaterials explored, scaffolds have been widely utilized due to their structural similarity to the natural extracellular matrix (ECM) and their ability to be synthesized from ECM-derived components[10–13]. Within this class of materials, methacrylated scaffolds have garnered significant interest due to their tunable mechanical and biochemical properties, making them highly suitable for cartilage tissue engineering applications[14–18]. Recently, Klara and colleagues successfully used methaycrylated forms of chitosan/gelatin/chondroitin sulfate for bone tissue regeneration[19]. Similarly, methacrylated chitosan and polyethylene glycol were recently used in injectable forms for cartilage regeneration[20].

Despite recent advancements in tissue engineering, replicating the intricate zonal architecture of native articular cartilage remains a critical challenge in scaffold design[21]. Articular cartilage is a highly specialized, multilayered tissue composed of four distinct zones; superficial, middle, deep, and calcified, each characterized

[1]Department of Medical Biology, Faculty of Medicine, Kırşehir Ahi Evran University, 40100 Kırşehir, Turkey. [2]Department of Nanotechnology and Nanomedicine, Graduate School of Science and Engineering, Hacettepe University, Ankara, Turkey. [3]Department of Chemistry, Biochemistry Division, Hacettepe University, 06230 Ankara, Turkey. [4]Biogenesis Biotechnology Co, 26190 Eskişehir, Turkey. ✉email: ekin.celik@ahievran.edu.tr

by unique cellular morphology, extracellular matrix composition, and collagen fiber orientation[22–24]. This zonal organization plays a pivotal role in maintaining the tissue's biomechanical integrity, facilitating smooth joint articulation, and providing resistance to compressive and shear forces.

The superficial zone, is the outermost layer of articular cartilage, composed of small and flattened chondrocytes embedded within a dense network of type II collagen fibers. These fibers are aligned parallel to the joint surface, enabling resistance to shear forces and facilitating the smooth gliding motion of the joint[25]. The intermediate zone or middle zone, located beneath the superficial zone, contains larger chondrocytes and randomly oriented collagen fibers that provide additional structural support and contribute to the cartilage's viscoelastic properties[26]. Deeper within the cartilage, the deep zone is characterized by tightly clustered chondrocytes and collagen fibers arranged perpendicular to the joint surface. This organization enhances the tissue's ability to withstand compressive forces, playing a crucial role in load distribution during weight-bearing activities[22,25]. At the interface between cartilage and bone lies the calcified zone, a transitional layer where the cartilage matrix becomes mineralized, and chondrocytes may undergo apoptosis. This layer serves as a crucial anchor, securing the cartilage to the underlying bone while facilitating force transmission across the osteochondral interface[27].

Conventional single-layer hydrogels are inherently limited in their ability to replicate the depth-dependent gradients in biochemical composition and mechanical properties that define native articular cartilage. To address this limitation, multilayered hydrogel systems with region-specific compositions have been explored to better emulate the structural and functional heterogeneity of the osteochondral interface[28–30].

In this study, we engineered a biomimetic multilayered hydrogel scaffold comprising methacrylated gelatin (GelMA), methacrylated chondroitin sulfate (CSMA), and polyethylene glycol dimethacrylate (PEGDMA), with nano-hydroxyapatite (nHA) incorporated into the deep layer to emulate the calcified cartilage interface. The construct was fabricated via sequential photopolymerization, enabling the formation of a stratified architecture with seamless interfacial bonding that recapitulates the zonal complexity of native articular cartilage. While the multilayered scaffold served as a successful proof-of-concept for spatially graded hydrogel integration, downstream biological and physicochemical characterizations were conducted on individually fabricated layers representing the superficial, middle, and deep cartilage zones. This approach was necessitated by the visual and mechanical homogenization of the multilayered construct post-crosslinking, which hindered precise spatial discrimination during analytical procedures. Despite this constraint, each formulation was rigorously evaluated for swelling behavior, enzymatic degradation kinetics, compressive modulus, cytocompatibility, zone-specific gene expression, and collagen type II deposition. These findings confirmed that each hydrogel layer maintained its intended functionality and structural identity, thereby validating the modular design strategy. Collectively, this work demonstrates the feasibility of constructing functionally graded scaffolds with zone-specific bioactivity and mechanical performance, offering a robust foundation for future translational applications in osteochondral tissue engineering. To our knowledge, this study is among the first to employ differential methacrylation and PEGDMA enhancement to fabricate zone-inspired hydrogel layers, enabling detailed analysis of their individual contributions to mimicking native cartilage microenvironments.

Materials & methods

Materials

Chondroitin sulfate, gelatin and methacrylate anhydride, Irgacure 2959 were purchased from Sigma (St. Louis, MO, USA). Fetal bovine serum, Dulbecco's Modified Eagle's Medium (DMEM) was purchased from Biological-Industries (Israel). Anti-collagen II antibody was purchased from Abcam (Cambridge, UK) and Alexa Fluor 488-conjugated goat anti-rabbit secondary antibody was purchased from Invitrogen, USA. All chemicals and reagents were used as received without any analytical purification. PEGDMA Mn ~ 550 was purchased from Merck, USA. Human chondrocytes (NHAC-Kn, CC-2550) and recommended chondrocyte medium (CC-3216) were purchased from Lonza, Switzerland.

CSMA and GelMA synthesis

A 10% (w/v) solution of Type A gelatin was prepared by dissolving gelatin in phosphate-buffered saline (PBS) to a final volume of 20 mL. The mixture was heated to 60 °C under constant stirring until complete dissolution was achieved. Methacrylic anhydride (MAA) was subsequently added dropwise at a rate of 100 µL/min in varying volumes (2–10 mL), while maintaining the reaction temperature below 60 °C to prevent gelatin denaturation. The reaction was allowed to proceed for 4 h under continuous stirring.

Following methacrylation, the reaction mixture was dialyzed against distilled water using a dialysis membrane with a molecular weight cut-off (MWCO) of 12–14 kDa at 40 °C for 4 days to remove unreacted reagents and byproducts. The dialyzed solution was then frozen and lyophilized for 5 days, yielding a white porous foam. The lyophilized product was stored at − 20 °C until further use.

To synthesize methacrylated chondroitin sulfate (CS-MA), a 25% (w/v) solution of chondroitin sulfate (CS) was prepared in phosphate-buffered saline (PBS). Methacrylic anhydride (MAA), in volumes ranging from 0.55 to 4.4 mL, was added dropwise under continuous stirring while maintaining the pH at 8.0 by the controlled addition of 5 N sodium hydroxide (NaOH). The reaction was carried out at room temperature for 3 h, followed by incubation at 4 °C for 24 h to ensure complete functionalization.

The resulting mixture was diluted with PBS and subjected to dialysis against distilled water using a 12–14 kDa molecular weight cut-off (MWCO) membrane at 40 °C for 4 days to remove unreacted MAA and byproducts. The dialyzed product was then frozen and lyophilized for 5 days, yielding a dry, porous material. The lyophilized CS-MA was stored at − 20 °C until further use in hydrogel formulation and characterization studies.

GelMA-CSMA hydrogel synthesis

To modulate the network density and mechanical properties of the GelMA-CSMA hydrogels and to simulate the stratified structure of native cartilage, poly (ethylene glycol) dimethacrylate (PEGDMA) was incorporated into the formulations. Various hydrogel compositions were prepared by adjusting the relative proportions of GelMA, CSMA, and PEGDMA, as detailed in Supplementary Table 1. A photoinitiator, 2-hydroxy-1-(4-(hydroxyethoxy) phenyl)-2-methyl-1-propanone (Irgacure 2959), was added to each formulation at a final concentration of 0.5% (w/v), and the mixtures were maintained at 60 °C to ensure complete dissolution and homogenization.

The prepolymer solutions were dispensed into 48-well tissue culture plates in defined volumes and subjected to ultraviolet (UV) light exposure at a wavelength of 365 nm for 10 min (intensity: 8–10 mW/cm^2) to initiate photo-crosslinking. Following polymerization, the hydrogels were transferred to phosphate-buffered saline (PBS) and stored under hydrated conditions for subsequent physicochemical and biological characterization.

Morphology

The morphological characterization of the micro- and nanoscale structure of the hydrogels was performed using scanning electron microscopy (SEM) (Quanta 250 FEG, FEI, USA). Prior to imaging, the samples were air-dried under ambient conditions and subsequently sputter-coated with a gold layer approximately 5 nm thick.

Swelling and in vitro degradation

Water retention, stability under physiological pH conditions, and enzymatic degradation profiles of the hydrogel constructs were systematically evaluated. Hydrogel samples weighing approximately 500 mg were immersed in phosphate-buffered saline (PBS, pH 7.4) and incubated at 37 °C in a water bath maintained at a constant shaking rate of 50 rpm. At predetermined time points, the samples were retrieved, gently blotted with lint-free tissue to remove surface moisture, and weighed to determine the water content. To assess enzymatic degradation, hydrogel samples were incubated under identical conditions in PBS supplemented with collagenase type II at a concentration of 2.5 U/mL. This enzymatic environment was employed to simulate in vivo matrix remodeling and evaluate the susceptibility of the hydrogels to proteolytic breakdown under physiologically relevant conditions[31].

Mechanical characterization

Mechanical characterization of the hydrogel constructs was conducted using a Universal Testing Machine (Zwick, Germany) equipped with a 100 N load cell. Cylindrical hydrogel samples with dimensions of approximately 10 mm in diameter and 10 mm in height were prepared and pre-equilibrated in phosphate-buffered saline (PBS, pH 7.4) for 24 h at 37 °C to ensure full hydration prior to testing.

Uniaxial compression tests were performed at a constant strain rate of 1 mm/min, with each sample compressed up to 20% of its original height. The compressive elastic modulus was calculated from the slope of the linear region of the resulting stress-strain curve, representing the elastic deformation range of the material. All measurements were conducted in triplicate ($n = 3$).

Development of a multi-layered model by stacking the hydrogels

To replicate the stratified architecture of native articular cartilage, a multilayered hydrogel model was developed by sequentially stacking distinct formulations representing the superficial, middle, deep and calcified zones. The polymer composition and concentrations used for each layer were specifically tailored to emulate the structural and mechanical characteristics of their corresponding native cartilage regions, as summarized in Table 1.

The superficial layer was formulated using chondroitin sulfate with a lower degree of methacrylation to promote higher water content and enhanced nutrient diffusion, reflective of the highly hydrated nature of the native superficial zone[32]. The middle layer incorporated gelatin with a high degree of methacrylation to impart increased crosslinking density and compressive resistance. The deep layer was composed of a densely crosslinked hybrid hydrogel matrix with reduced water content, designed to support load-bearing function and improve mechanical strength at the osteochondral interface. To mimic the calcified cartilage zone, 5% (w/v) nano-hydroxyapatite (nHA) was incorporated into the deep layer formulation, enhancing mineral content and stiffness to more closely resemble the osteochondral interface and promote integration with subchondral bone[33].

In all formulations, 2-hydroxy-1-(4-(hydroxyethoxy) phenyl)-2-methyl-1-propanone (Irgacure 2959) was employed as the photoinitiator at a concentration of 0.5% (w/v). Calcified, deep, middle and superficial layers were sequentially cast into silicone molds and photo-crosslinked under ultraviolet (UV) light at 365 nm for 10 min per layer, ensuring interfacial bonding and structural continuity between layers.

Gelation efficiency

Gelation efficiency was determined by calculating the ratio of the dry weight of hydrogels remaining after lyophilization to the initial solid content introduced into the reaction medium prior to crosslinking. Prepolymer

Cartilage zone	Base polymer formulation (w/v)	PEGDMA concentration (w/v)	Bioactive additive (w/v)	Total solid content
Superficial	15% (CSMA2 + GelMA2)	5%	–	20%
Middle	15% (CSMA2 + GelMA3)	5%	–	20%
Deep	20% (CSMA2 + GelMA3)	15%	–	35%
Calcified	20% (CSMA2 + GelMA3)	15%	5% nHA	35% + nHA

Table 1. Polymer compositions and concentrations used for the fabrication of zone-specific hydrogels.

solutions were prepared according to the specified formulations and subjected to UV-induced crosslinking (365 nm, 10 min). The resulting hydrogels were incubated in phosphate-buffered saline (PBS, pH 7.4) at 37 °C for 24 h to remove any unreacted or loosely bound components.

After incubation, the hydrogels were frozen, lyophilized, and weighed. Gelation efficiency (%) was calculated using the following formula:

$$\text{Gelation Efficiency}\,(\%) = \left(\frac{W_{\text{dry hydrogel}}}{W_{\text{initial solids}}}\right) \times 100$$

where $W_{\text{dry hydrogel}}$ represents the dry weight of the lyophilized gel, and $W_{\text{initial solids}}$ corresponds to the total mass of polymer initially added to the reaction mixture. All experiments were conducted in triplicate, and results are expressed as mean ± standard deviation.

Chondrocyte encapsulation

Human chondrocytes were encapsulated within the hydrogel matrix during the gelation process to simulate the native cartilage microenvironment. While the multilayered architecture was fabricated and characterized structurally, cell culture studies were performed on each layer separately to assess their zone-specific bioactivity. Immediately prior to UV-induced crosslinking, human chondrocytes (3×10^5 cells per well) were incorporated into the prepolymer solutions. Crosslinking was initiated without delay to ensure uniform cell encapsulation and structural integrity of the hydrogel constructs. Following photopolymerization, culture medium was added, and the cell-laden hydrogels were maintained under standard culture conditions for 7, 14, and 28 days.

Cell viability

The cytocompatibility of the hydrogel formulations was evaluated using the WST-1 assay on human chondrocytes. Cells were seeded into 96-well tissue culture plates at a density of 5×10^4 cells per well and allowed to reach approximately 70% confluency. Subsequently, hydrogel extracts were applied at concentrations of 30, 15, and 5 µg/mL, with each condition tested in triplicate. The cells were incubated with the hydrogels for 24 and 48 h. Control wells received culture medium without hydrogel extracts.

Following incubation, 10 µL of WST-1 reagent was added to each well, gently mixed for 1 min, and incubated at 37 °C for an additional 2 h. Metabolically active cells reduce the WST-1 reagent to a water-soluble formazan dye, which produces a yellow color. The absorbance was measured using a microplate reader in the range of 420–480 nm, with the intensity directly correlating to the number of viable cells. Wells with non-viable or dead cells exhibited minimal to no color development.

Gene expression analysis

Gene expression levels of the cells were determined 28 days post-encapsulation using the Comparative Ct (ddCt) method. The gene expression of chondrocytes was normalized to the GAPDH gene and analyzed using an Applied Biosystems QuantStudio 5 Real Time PCR system. The gene expression analysis included a total of four different hydrogel formulations. Statistical analysis was performed on three biological replicates ($n = 3$), with each measured in technical triplicate. In accordance with the experimental design, RNA isolation, genomic DNA removal, complementary DNA (cDNA) synthesis and quantitative real-time PCR (qRT-PCR) analysis the following sequential procedures were performed. Primers used in the experiment are given in Supplementary Table 2.

Florescence imaging

Hydrogel-embedded chondrocytes were cultured for 7, 14 and 28 days after which samples were washed twice with phosphate-buffered saline (PBS) and fixed with 4% paraformaldehyde (PFA) at room temperature for 30 min. Following fixation, samples were rinsed three times with PBS, permeabilized with 0.2% Triton X-100 in PBS for 15 min, and subsequently blocked using 3% bovine serum albumin (BSA) in PBS at room temperature for 60 min. After blocking, samples were incubated overnight at 4 °C with rabbit anti-collagen type II primary antibody (1:200 dilution in 1% BSA/PBS; Abcam) Following incubation, hydrogels were thoroughly washed three times in PBS to remove unbound antibodies. Samples were then incubated with Alexa Fluor 488-conjugated goat anti-rabbit secondary antibody (1:400 dilution in 1% BSA/PBS; Invitrogen) at room temperature for 1 h in the dark. After final washes (3 × 5 min) with PBS, samples were counterstained with DAPI (1 µg/mL in PBS; Invitrogen) for nuclear visualization[34]. Fluorescent images were captured using a confocal laser scanning microscope (e.g., Zeiss LSM series).

Statistical analysis

All experiments were conducted in triplicate unless otherwise stated, and results are presented as mean ± standard deviation (SD). Statistical analyses were performed using GraphPad Prism v.10 (GraphPad Software, USA). Data were assessed for normality using the Shapiro–Wilk test. Student's *t*-test, Mann–Whitney U test was applied. For comparisons involving more than two groups, one-way analysis of variance (ANOVA) followed by Tukey's post hoc test was performed. A p-value of < 0.05 was considered statistically significant. Asterisks were used to indicate statistical significance as follows: $p < 0.05$ (*), $p < 0.01$ (**), $p < 0.001$ (***), $p < 0.0001$ (****), and "ns" denotes non-significant differences.

Results & discussion

Methacrylation of CSMA and GelMA hydrogels

Methacrylation of chondroitin sulfate (CS) using methacrylic anhydride (MAA) involves the esterification of hydroxyl (–OH) groups present on the CS backbone. Each disaccharide unit of CS possesses three hydroxyl groups that are theoretically available for functionalization, allowing for the incorporation of methacrylate moieties along the polymer chain[35]. Under the assumption of complete methacrylation, the degree of substitution would be 3, corresponding to a theoretical maximum conversion of 100%.

The proton nuclear magnetic resonance (^{1}H-NMR) spectra of methacrylated chondroitin sulfate samples provide insight into the extent of methacrylation (Supplementary Fig. 1). The characteristic vinyl protons of the methacrylate group (C=CH_2) appear in the chemical shift range of 5.5–6.0 ppm. These peaks were observed at low intensity in the CSMA1 sample, which was synthesized using a low concentration of MAA. In contrast, the intensity of these peaks increased in the CSMA2 and CSMA3 samples, indicating a higher degree of methacrylation with increasing MAA concentration.

Additionally, the degree of methacrylation can be semi-quantitatively assessed by comparing the integration of the methyl protons of the methacrylate group (~ 1.84 ppm) to that of the methyl protons in the native amide group (~ 1.91 ppm). As noted earlier, the theoretical maximum for this ratio is 3. The calculated degrees of methacrylation based on this ratio are presented in Supplementary Table 3. The methacrylation of gelatin using methacrylic anhydride (MAA) occurs primarily through the reaction of the free amine (-NH_2) groups on lysine residues within the gelatin polypeptide chain[36]. These amine groups act as nucleophiles, reacting with MAA via nucleophilic substitution to form covalent bonds that introduce methacrylate functional groups.

The degree of methacrylation was quantified by analyzing the ^{1}H-NMR spectra, based on the ratio of the vinyl proton signal of the methacrylated amines (~1.80 ppm) to the combined signal intensity of the non-methacrylated amine protons observed in the same region and at approximately 2.9 ppm. This ratio provides an estimate of the extent of functionalization. The calculated degrees of methacrylation for each sample, derived from this analysis, are presented in Supplementary Table 3.

The proton nuclear magnetic resonance (^{1}H-NMR) spectra of the methacrylated gelatin samples reveal characteristic peaks in the region of 5.5–6.0 ppm, corresponding to the vinyl protons (C=CH_2) of the methacrylate groups (Supplementary Fig. 2). These peaks were observed with low intensity in the GelMA1 sample, which was synthesized using a low concentration of methacrylic anhydride. In contrast, the intensity of the vinyl proton signals increased markedly in the GelMA2 and GelMA3 samples, indicating a higher degree of methacrylation with increasing anhydride concentration.

Swelling

Water content was evaluated by weighing the hydrogels in their fully swollen state, followed by lyophilization to obtain the dry weight. The water content was expressed as the percentage of retained water, calculated using the formula:

$$\text{water content} = 100\% \times \frac{(m_{\text{swollen}} - m_{\text{dry}})}{m_{\text{dry}}}$$

Hydrogel swelling behavior was assessed over a 14-day immersion period in phosphate-buffered saline (PBS, pH 7.4), as detailed in Supplementary Fig. 3. All hydrogel formulations maintained their structural integrity throughout the duration of the study, with no evidence of hydrolytic degradation observed in any of the UV-crosslinked groups. Within the CSMA-based hydrogels, higher swelling ratios were recorded in formulations lacking PEGDMA, indicating a looser crosslinking network ($p < 0.05$). In contrast, PEGDMA incorporation in GelMA-based hydrogels led to increased swelling capacity relative to their non-modified counterparts, likely due to enhanced hydrophilicity and network expansion ($p < 0.05$). This divergence can be attributed to the distinct molecular architectures and functional group densities of the base polymers. CSMA, derived from chondroitin sulfate, contains a highly charged, sulfated polysaccharide backbone with abundant hydrophilic moieties[37]. Upon PEGDMA incorporation, the formation of a denser and more tightly crosslinked network restricts chain mobility and reduces the osmotic driving force for water uptake, resulting in decreased swelling. In contrast, GelMA possesses a protein-based backbone with a lower inherent charge density and more flexible network configuration. The addition of PEGDMA, which is hydrophilic and flexible, contributes additional water-binding sites and expands the mesh size in the GelMA matrix, thereby enhancing water absorption and swelling capacity[38].

Mechanical characterization

Mechanical characterization of the hydrogels was carried out through uniaxial compression testing to assess their structural integrity and stiffness. The compressive modulus, which reflects the material's resistance to deformation under load, is particularly important for mimicking the mechanical environment of native cartilage tissue. Since articular cartilage exhibits significant load-bearing function in vivo, evaluating the compressive properties of the hydrogels provides critical insight into their potential applicability in cartilage tissue engineering[39]. Compressive moduli of synthesized hydrogels are given in Supplementary Table 4.

An increase in the compressive modulus of chondroitin sulfate-based hydrogel structures was observed with higher degrees of methacrylation, indicating a positive correlation between crosslinking density and mechanical stiffness. For the CSMA1 sample, which exhibited a methacrylation degree of 13%, the compressive modulus was measured at 3.26 kPa. When the methacrylation degree was increased to 22%, this value rose approximately 12-fold, reaching 38.5 kPa. However, mechanical testing could not be performed on the CSMA sample with the highest methacrylation level, as structural cracking and deformation occurred during the PBS immersion phase,

compromising the integrity of the sample. Although the ~20 kPa increase in compressive modulus observed between the first two degrees of methacrylation in GelMA samples was not statistically significant, a substantial increase was noted in the GelMA3 sample, which exhibited the highest methacrylation degree (88%), with a compressive modulus reaching 180 kPa.

Following PEGDMA incorporation, an enhancement in mechanical strength was observed across all hydrogel samples. The most pronounced increase occurred in the CSMA1 sample, where the compressive modulus reached 52.1 kPa. In the CSMA2 sample, this value increased more than threefold, reaching 141 kPa. For the PEGDMA-incorporated GelMA samples, the compressive modulus values increased by approximately 1.5- to 2-fold compared to their non-incorporated counterparts, with final values of 209, 232, and 268 kPa for GelMA1-PEGDMA, GelMA2-PEGDMA, and GelMA3-PEGDMA, respectively. These values fall within the lower range of native articular cartilage, which typically exhibits compressive moduli between 240 and 1000 kPa depending on anatomical location and testing condition[39–41]. This suggests that PEGDMA-enhanced hydrogels demonstrate improved mechanical resilience and may serve as suitable candidates for load-bearing tissue engineering applications such as cartilage regeneration, consistent with previous findings highlighting PEGDMA's role in reinforcing hydrogel networks and enhancing compressive strength in composite scaffolds[42].

Morphology

To evaluate the microstructural features of the synthesized hydrogels, scanning electron microscopy (SEM) was performed on freeze-dried samples. SEM analysis revealed that all CSMA and GelMA-based hydrogel formulations exhibited interconnected porous architectures, a critical feature for facilitating cell infiltration, nutrient diffusion, and tissue integration in cartilage tissue engineering[43–45].

CSMA1 and CSMA2 hydrogels displayed relatively uniform and well-defined pores, ranging from 20 to 150 µm (Supplementary Fig. 4). In contrast, the CSMA3 formulation exhibited reduced pore uniformity and thinner pore walls, likely due to excessive crosslinking associated with its higher methacrylation degree. The incorporation of PEGDMA into CSMA2 resulted in a denser crosslinking network, as evidenced by a slight reduction in pore wall thickness, although the overall porous morphology was largely preserved.

SEM images of GelMA-based hydrogels (Supplementary Fig. 5) similarly confirmed well-distributed porous structures, with pore sizes ranging from 50 to 200 µm, dimensions considered optimal for chondrogenic cell activity and tissue regeneration[46–49]. Notably, GelMA-based hydrogels modified with PEGDMA exhibited superior pore interconnectivity, narrower pore size distribution, and enhanced structural stability, indicative of a more complex and mechanically resilient network architecture. These constructs demonstrated larger, more uniform, and well-interconnected pores compared to their CSMA-based counterparts, highlighting their suitability for load-bearing applications in osteochondral tissue regeneration. This favorable microarchitecture can be attributed to the relatively flexible and loosely packed nature of the GelMA-PEGDMA network, which facilitates the formation of open and well-defined porous structures during photopolymerization[50].

In contrast, CSMA hydrogels displayed denser and more variable pore morphologies, where porosity was highly dependent on methacrylation degree and crosslinking density. The inherently stiffer polysaccharide backbone of CSMA, coupled with a high density of reactive functional groups, promotes tighter network packing and reduced pore formation upon PEGDMA incorporation. As a result, CSMA-based scaffolds tended to form smaller pores with thinner walls, reflecting a more brittle and compact network[35].

These observations underscore the pivotal role of base polymer chemistry in dictating the outcome of crosslinker interactions. By strategically modulating polymer-crosslinker combinations, it is possible to fine-tune both hydration characteristics and internal architecture to meet the specific mechanical and biological demands of each cartilage zone. Such material-dependent design flexibility is instrumental in developing structurally graded scaffolds that accurately recapitulate the native heterogeneity of articular cartilage.

Based on prior material-specific characterization results, specific compositions were strategically selected to represent each zone of native articular cartilage in a biomimetic multilayered construct (Fig. 1a). For the superficial zone, a formulation comprising 15% (w/v) of a CSMA2 and GelMA2 blend, supplemented with 5% PEGDMA (total 20% solid content), was selected to emulate the highly hydrated, low-density matrix that facilitates lubrication, nutrient exchange, and resistance to shear forces at the articular surface. The middle zone, which serves as a transitional region providing moderate compressive strength and matrix density, was represented using the formulation (15% CSMA2 + GelMA3 with 5% PEGDMA), ensuring compositional continuity while maintaining functional distinction.

To mimic the deep cartilage zone, which is characterized by its role in resisting compressive loads and anchoring the tissue to the calcified interface, a more mechanically robust formulation was employed. This consisted of 20% (w/v) of a CSMA2 and GelMA3 blend, enriched with 15% PEGDMA to increase crosslinking density and reduce swelling. The denser configuration is advantageous for the deep zone, which is characterized by high matrix density, reduced porosity, and increased load-bearing capacity[51].

Finally, to simulate the calcified cartilage zone at the osteochondral interface, the same dense formulation was further reinforced with 5% (w/v) nano-hydroxyapatite (nHA), enhancing stiffness and promoting mineralization to facilitate integration with the underlying subchondral bone.

Overall, the formulations were designed with progressively increasing solid content and PEGDMA concentration from the superficial to the calcified zone, in alignment with the native biochemical and biomechanical gradients of articular cartilage. This rational design strategy facilitates the development of a structurally and functionally graded hydrogel scaffold, in which the upper layers, characterized by higher porosity and hydration, are tailored to promote early-stage cell infiltration, nutrient diffusion, and extracellular matrix deposition, whereas the deeper layers offer enhanced mechanical integrity and matrix density to withstand compressive loads and support long-term osteochondral regeneration.

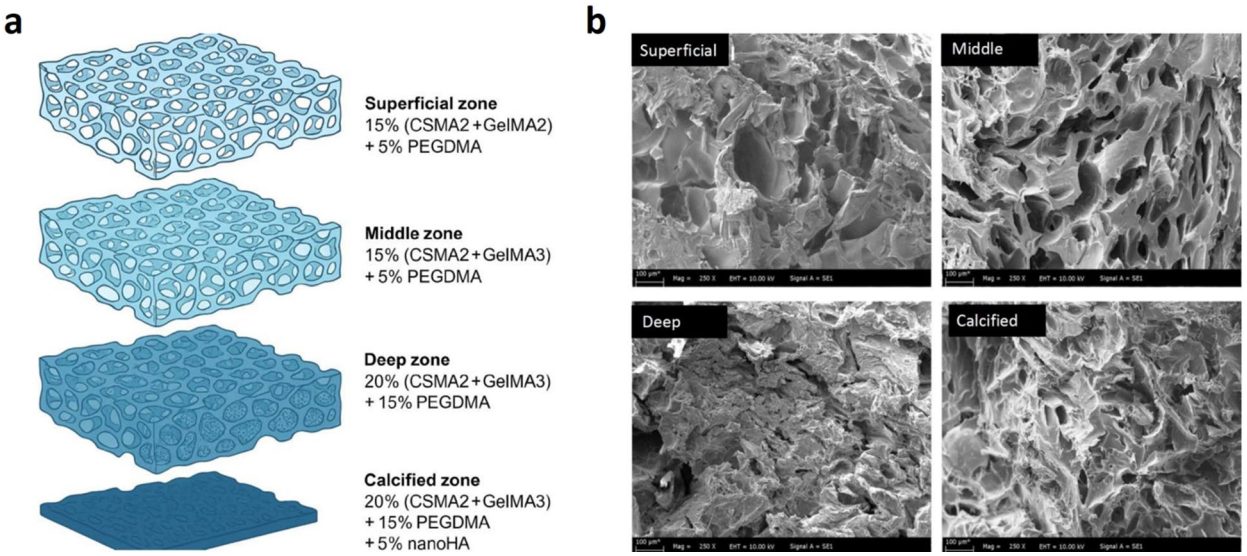

Fig. 1. (**a**) Schematic representation of the multilayered osteochondral scaffold, composed of sequentially photopolymerized hydrogels tailored to mimic the native zonal architecture of articular cartilage. (**b**) Scanning electron microscopy (SEM) images of hydrogel layers designed to mimic distinct cartilage zones, captured at 250× magnification.

SEM was employed to examine the microstructural features of the distinct hydrogel layers, particularly focusing on their internal porosity and morphological transitions across the construct. Figure 1b presents the cross-sectional images of the hydrogel layers obtained after lyophilization, revealing the internal porous structures of each layer. A distinct gradation in pore morphology is observed across the layers, with pore size decreasing progressively from the superficial to the calcified zone. Quantitative analysis confirmed this gradient, with mean pore diameters measuring 124.0 ± 15.9 µm in the superficial zone, decreasing to 92.4 ± 10.6 µm in the middle zone, 62.9 ± 8.4 µm in the deep zone, and 31.0 ± 7.0 µm in the calcified zone (Supplementary Fig. 6). This reduction in pore diameter correlates with the increasing crosslinking density and total solid content applied in the deeper layers of the construct. The tighter and more compact pore architecture in the lower layers reflects a design strategy intended to mimic the natural transition of the extracellular matrix from the highly porous superficial cartilage zone to the dense, mineralized calcified zone. These morphological differences further validate the zonal hydrogel design and demonstrate the ability to control microstructural features through compositional tuning.

Design and morphological evaluation of a stacked hydrogel structure

To investigate the feasibility of constructing zonal scaffolds for cartilage tissue engineering, a multilayered hydrogel was fabricated by stacking CSMA, GelMA and PEGDMA formulations as mentioned, representing the superficial, middle, deep and calcified zones of native cartilage, respectively. Optical and scanning electron microscopy (SEM) images were obtained to evaluate the structural integrity and morphological distinction between layers (Fig. 2).

SEM image revealed that stacked hydrogel structure remained intact, and no delamination, breakage, or rupture between the layers. Figure 2b presents the optical image of the stacked hydrogel construct, which was fabricated by sequentially layering and crosslinking CSMA2 (colored with yellow dye, though not clearly visible in the image), GelMA3 (dark blue), and a CSMA2-GelMA3 mixture (red–purple). Following crosslinking, the construct demonstrated high mechanical stability in PBS, with no visible deformation or structural compromise during incubation.

Although whole-construct mechanical testing was not performed, the cross-sectional SEM analysis demonstrated seamless interfacial bonding with no delamination, confirming that sequential photopolymerization effectively integrated the layers. This structural continuity serves as a compelling proof-of-concept for the successful fabrication of cohesive, mechanically graded scaffolds. Importantly, the individual hydrogel formulations selected to mimic each cartilage zone, specifically CSMA2 and GelMA3 variants, were comprehensively characterized in terms of their swelling profiles, microstructural features, mechanical properties, and in vitro biological performance. These data validate the functional suitability of each layer and support their integration into a composite scaffold that recapitulates the hierarchical organization of native articular cartilage.

Similarly, biological evaluations were conducted on the individual hydrogel formulations rather than the fully integrated scaffold. This decision was based on a practical limitation encountered during post-fabrication handling: once photo-crosslinked and hydrated, the layered hydrogel became macroscopically homogeneous in appearance and texture, making it technically challenging to distinguish and spatially isolate the individual layers during downstream analyses such as gene expression profiling or immunostaining. As accurate attribution

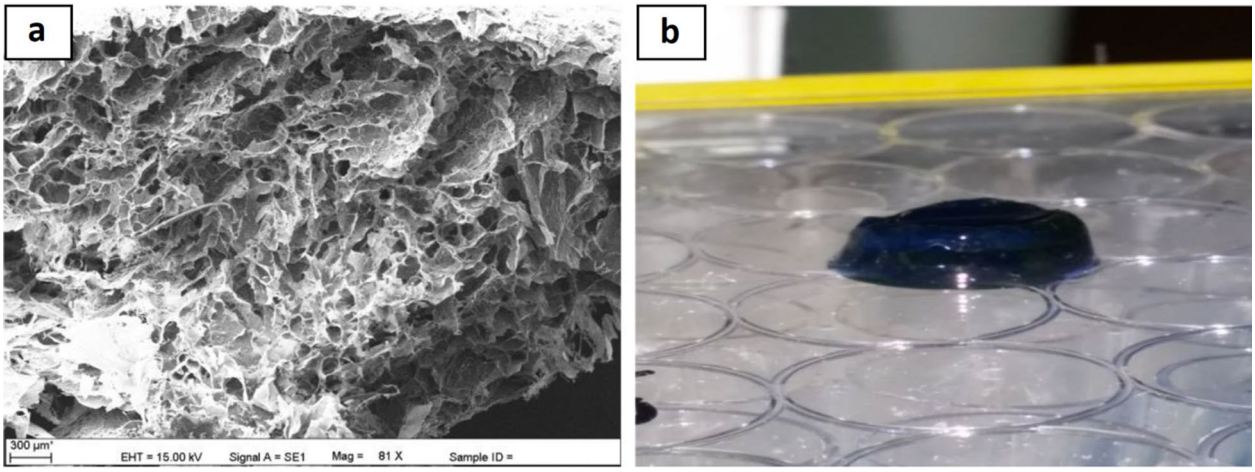

Fig. 2. Morphological proof-of-concept of the multilayered hydrogel structure designed to mimic the zonal architecture of native cartilage. (**a**) Cross-sectional SEM image (81× magnification). (**b**) Optical image of the stacked hydrogel after fabrication and crosslinking.

of biological responses to specific zones is critical for validating the functional mimicry of the scaffold, we prioritized layer-by-layer characterization. Future studies will address this limitation through the incorporation of zone-specific fluorescent tags, histological tracking methods, or embedded spatial markers to enable precise localization of cellular activity within the multilayered construct.

Gelation efficiency

Gelation efficiency was calculated as the ratio of the dry weight of hydrogels remaining after lyophilization to the initial solid content introduced into the reaction medium prior to gelation. The results demonstrated a high degree of correlation between the expected and measured solid contents for all groups (Supplementary Fig. 7). Statistical analysis revealed no significant difference between the superficial and middle layers ($p > 0.05$), as well as between the deep and calcified layers ($p > 0.05$), indicating consistent gel formation in these paired regions. However, all other intergroup comparisons showed statistically significant differences ($p < 0.001$), confirming that variations in formulation composition were accurately reflected in the resulting solid content. The results showed that gelation efficiency exceeded 95% in both the superficial and middle layer formulations, which contained a total solid content of 20%. In contrast, efficiency decreased to approximately 80% in the deep and calcified layer formulations, where the total solid content was increased to 35%. This reduction is likely attributed to the increased material density, which may hinder the uniform penetration of ultraviolet light within the same exposure duration, thereby limiting complete crosslinking in more concentrated formulations.

Water retention and degradation

The water retention (swelling) properties of hydrogels are critical parameters influencing their performance in tissue engineering applications[52]. To evaluate these characteristics, lyophilized hydrogel samples were rehydrated in phosphate-buffered saline (PBS) for 1 h, and their water uptake capacities were quantified. The swelling capacities of the hydrogel layers, expressed as percentage increase in weight after PBS immersion, are shown in Fig. 3a. A clear decreasing trend was observed from the superficial to the calcified zone, consistent with increasing crosslinking density and solids content. The superficial layer exhibited the highest swelling ratio (~ 261%), followed by the middle (~ 221%), deep (~ 176%), and calcified (~ 165%) layers. Statistical analysis confirmed that all intergroup differences were highly significant ($p < 0.0001$), indicating that variations in formulation composition and network density were effectively translated into distinct swelling behaviors. This gradient is in alignment with the functional heterogeneity observed in native articular cartilage tissue.

The degradation profiles of the hydrogel structures over a 14-day period in the presence of collagenase are presented in Fig. 3b. As shown in the figure, the superficial and middle layer formulations, both containing comparable total solid content, exhibited similar overall degradation behavior. However, the middle zone, which incorporated gelatin with a higher degree of methacrylation than the superficial layer, demonstrated increased resistance to enzymatic degradation, retaining approximately 10% more of its mass by day 14. In contrast, the degradation profile of the deep zone hydrogel, which used the same degree of methacrylated gelatin as the middle layer but with a higher total solid content (35%), differed significantly from the upper layers. This formulation exhibited a more sustained, linear degradation trend, particularly from day 3 onward, and retained over 60% of its initial mass at the end of the study period. These results highlight the critical roles of both methacrylation degree and solid content in modulating enzymatic degradation behavior, offering important insights for the design of zone-specific, temporally tunable scaffolds in cartilage tissue engineering. The use of collagenase in this study provides physiologically relevant conditions, as it mimics matrix metalloproteinase activity involved in native cartilage remodeling and degradation processes.

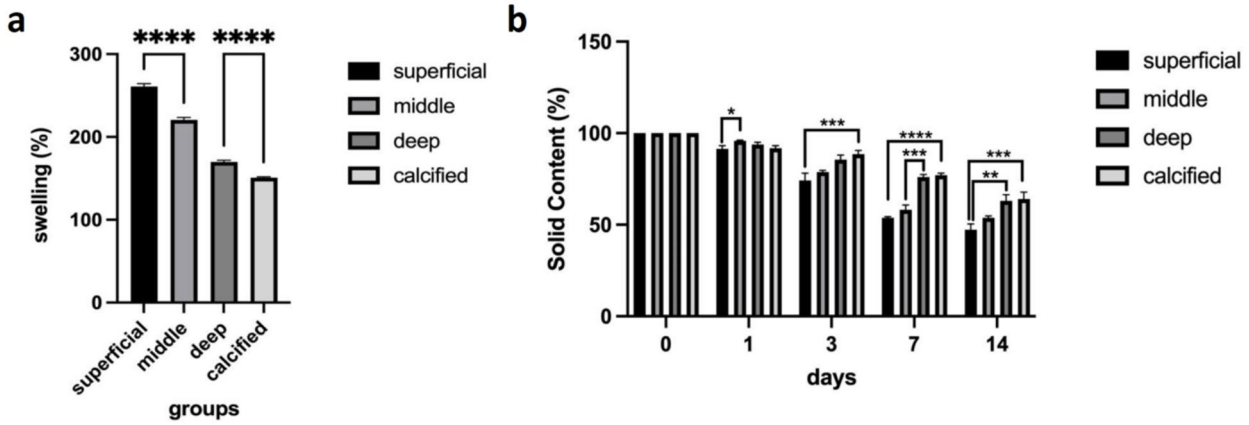

Fig. 3. (**a**) Swelling degrees of hydrogels, (**b**) Degradation profiles of hydrogels in the presence of collagenase over a 14-day period.

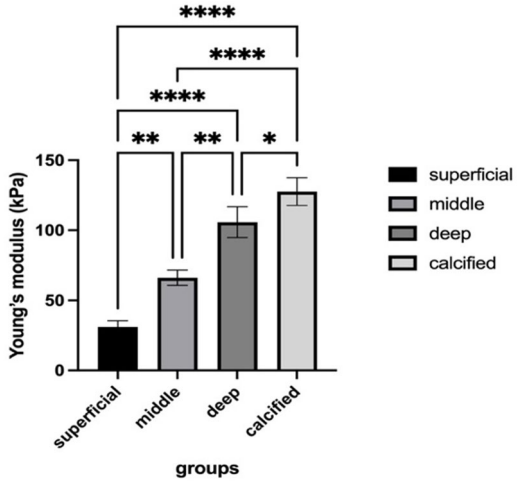

Fig. 4. Young's modulus values of hydrogels.

Mechanical testing

The mechanical properties of the four distinct hydrogel layers were evaluated using uniaxial compression testing. Young's modulus values were calculated from the linear region of the stress-strain curves, specifically within the 5–10% strain range. A clear increasing trend in stiffness was observed from the superficial to the calcified zone, reflecting the intended gradient in crosslinking density and solid content. The superficial layer exhibited the lowest modulus (~ 31 kPa), while the middle, deep, and calcified layers showed progressively higher values of approximately 66 kPa, 106 kPa, and 128 kPa, respectively (Fig. 4). Statistical analysis revealed that all intergroup differences were significant, with $p < 0.01$ between superficial-middle and superficial-deep layers, $p < 0.0001$ between superficial-calcified, middle-deep, and middle-calcified layers, and $p < 0.05$ between the deep and calcified layers. Stress-strain curves are given in Supplementary Fig. 8.

While the compressive moduli of the fabricated hydrogel layers (ranging from ~ 31 kPa in the superficial zone to ~ 128 kPa in the calcified zone, with optimized GelMA3-PEGDMA formulations reaching ~ 268 kPa) fall within the lower range of mature native articular cartilage (typically 240–1000 kPa), this stiffness range represents a strategic balance between mechanical integrity and biological permissiveness[53]. In hydrogel design, increasing stiffness to match mature tissue typically requires excessive crosslinking density or solid content, which can detrimentally impact pore interconnectivity and hinder nutrient diffusion. Our SEM analysis confirmed that formulations with the highest methacrylation degrees, while mechanically superior, resulted in reduced pore uniformity and wall thickness. Consequently, the selected formulations prioritize an open porous architecture (50–200 µm) to facilitate cell infiltration and metabolic activity, as evidenced by the high cell viability (> 95%) observed in the WST-1 assays across all zones. Furthermore, these hydrogel constructs are designed as temporary regenerative templates rather than permanent prosthetic replacements; the mechanical properties are expected to improve progressively in vivo as the encapsulated chondrocytes deposit functional extracellular matrix, a process already initiated in vitro as demonstrated by the robust, zone-specific Collagen type II deposition observed by Day 28.

Cytotoxicity

The in vitro cytotoxicity assessment of the methacrylated precursors, GelMA, CSMA and PEGDMA utilized in the fabrication of zone-specific hydrogel formulations is presented in Supplementary Fig. 9. Neither material exhibited cytotoxic effects, as evidenced by the absence of statistically significant differences in cell viability between treated and control groups. These results confirm the effective removal of residual methacrylic anhydride and any by-products generated during the methacrylation of gelatin and chondroitin sulfate, following rigorous purification procedures. The high levels of cell viability observed validate the cytocompatibility of these modified biopolymers, thereby ensuring their safe integration into hydrogel systems intended for cartilage tissue engineering applications.

Gene expression

After 28 days of culture in the zone-specific hydrogel constructs, gene expression analysis revealed distinct spatial profiles that closely resemble the transcriptional stratification of native articular cartilage (Fig. 5). COL2A1 (type II collagen) expression was significantly upregulated in the middle zone-mimicking hydrogels, reaching levels approximately 2.5-fold higher than in the superficial zone and markedly exceeding expression observed in both the deep and calcified groups ($p < 0.0001$) (Fig. 5a). This peak in COL2A1 expression reflects the biosynthetic activity typically associated with transitional-zone chondrocytes, which are primarily responsible for maintaining the fibrillar collagen matrix necessary for mechanical resilience[22].

Similarly, ACAN (aggrecan) expression followed a comparable zonal pattern, with significantly higher expression in the middle and deep hydrogel regions compared to the superficial and calcified groups ($p < 0.0001$). These results are in line with the functional demands of the middle zone, where proteoglycan-rich extracellular matrix supports tissue hydration and compressive load dissipation. The observed decline in ACAN expression in the calcified hydrogel is consistent with the onset of chondrocyte hypertrophy and matrix mineralization, where proteoglycan production is typically reduced (Fig. 5b).

In contrast, Fig. 5c shows COL10A1 (type X collagen), a well-established marker of chondrocyte hypertrophy, displayed a progressive and statistically significant increase across the hydrogel zones, culminating in the highest expression within the calcified-mimicking region ($p < 0.0001$)[54]. This spatial distribution suggests a successful phenotypic transition of chondrocytes toward a terminally differentiated, hypertrophic state in response to cues provided by the calcified microenvironment. The observed low expression of COL10A1 in the superficial and middle zones is a crucial finding, suggesting the maintenance of a stable, non-hypertrophic chondrocyte phenotype in these regions[55–57]. While all 3D hydrogel culture systems inherently possess subtle nutrient and oxygen gradients, our WST-1 assay confirmed high cell viability (> 95%) across all zones after 28 days. This high viability directly refutes the presence of detrimental nutrient deprivation or severe diffusion limitation that would lead to cell mortality. Therefore, the low COL10A1 is interpreted not as a failure of diffusion, but as successful zonal phenotypic control, where the specific material composition of the superficial layer supports the desired non-hypertrophic phenotype, maintaining cell function without the terminal differentiation observed in the nHA-enriched deep zone.

Together, these findings confirm that the engineered hydrogel system supports region-specific chondrogenic differentiation, with molecular signatures reflective of native cartilage zonation. The upregulation of COL2A1 and ACAN in the middle and deep zones, coupled with the selective enrichment of COL10A1 in the calcified zone, demonstrates the scaffold system's ability to recapitulate the hierarchical structure and function of articular cartilage. These results are consistent with prior reports on zonal matrix composition and gene expression in

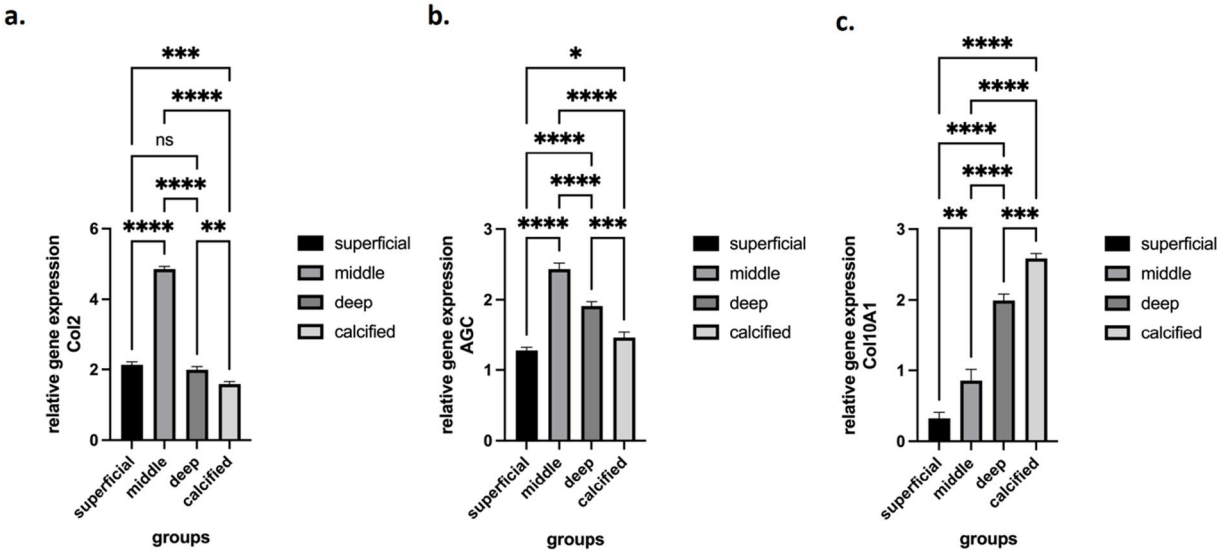

Fig. 5. Gene expression analysis of chondrocytes cultured within zonal hydrogel layers after 28 days (**a**) COL2A1 (**b**) ACAN (**c**) COL10A1 ($n = 3$).

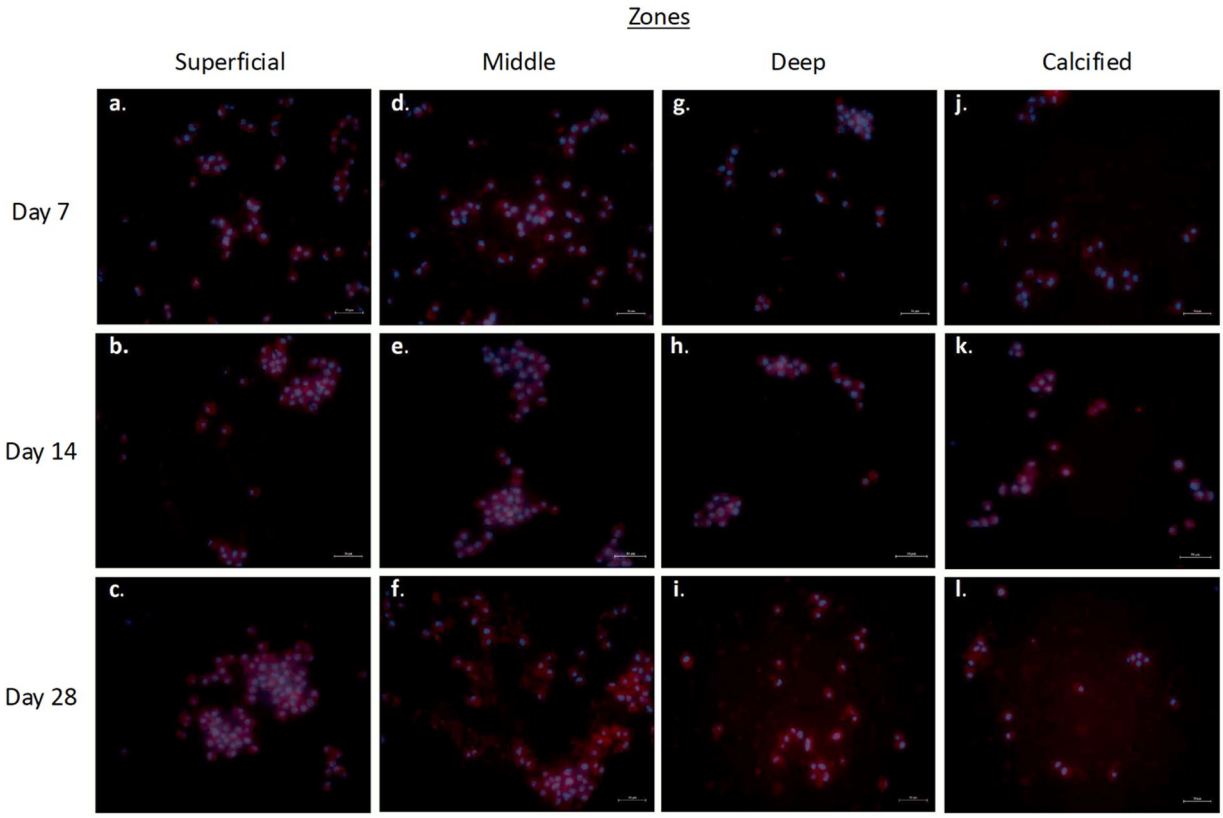

Fig. 6. Representative fluorescence microscopy images showing Collagen II (red) and nuclei (DAPI, blue) staining of chondrocytes in different hydrogels. Cells were fixed and stained on Day 7, 14 and 28 of cell culture. Images a-l corresponds to the following groups, respectively: (**a**–**c**) superficial zone day 7 (**a**), day 14 (**b**), day 28 (**c**), (**d**–**f**) middle zone day 7 (**d**), day 14 (**e**), day 28 (**f**), (**g**–**i**) deep zone day 7 (**g**), day 14 (**h**), day 28 (**i**), (**j**–**l**) deep zone day 7 (**j**), day 14 (**k**), day 28 (**l**).

both native and engineered cartilage and highlight the system's promise for biomimetic osteochondral tissue engineering[58–61].

Collagen II staining

Temporal analysis of collagen type II immunofluorescence staining was performed at days 7, 14, and 28 to assess chondrogenic progression within the zonal hydrogel constructs, representative images are given in Fig. 6. At day 7, weak perinuclear staining became evident, particularly in the superficial and middle zones, indicating the onset of chondrogenic differentiation. The signal remained sparse and localized, with limited extracellular distribution. At day 14, collagen type II expression markedly increased in the superficial and middle layers, with more widespread pericellular and early extracellular matrix deposition. In contrast, the deep and calcified zones still exhibited lower signal intensity, consistent with delayed or limited chondrogenesis in denser, more crosslinked environments.

By day 28, strong and continuous collagen type II staining was observed in the superficial and middle zone constructs, forming a well-organized extracellular matrix that closely resembled native hyaline cartilage. The most intense and widespread collagen type II staining was observed in the middle zone, indicating a higher level of chondrogenic activity and matrix deposition in this region compared to the other zones. The signal was more diffuse and extended beyond the pericellular space for all hydrogels, indicating advanced matrix maturation[62] Semi-quantitative analysis confirmed a statistically significant and zone-dependent increase in Collagen Type II fluorescence intensity, which is detailed quantitatively in Supplementary Fig. 10. Although the deep and calcified zones continued to show lower expression, a modest increase was noted compared to earlier timepoints, suggesting a spatial and temporal gradient of chondrogenesis across the construct. These findings are in line with the gene expression results and confirm not only the zonal differentiation potential of the hydrogels but also the progressive maturation of cartilage-like matrix over time[61,63–65].

While this study demonstrates the feasibility of a biomimetic stratified hydrogel system for osteochondral tissue engineering, we acknowledge certain limitations that should be addressed in future research. A primary limitation of this study was the macroscopic homogenization of the multilayered construct post-crosslinking, which, while indicating seamless integration, prevented spatial discrimination during whole-construct biological analysis. Consequently, biological characterizations were restricted to individual layers, precluding the assessment of cellular cross-talk and nutrient gradients inherent to the intact stratified scaffold. Furthermore,

although the compressive moduli fell within the lower range of native tissue to prioritize pore interconnectivity and cell viability, the constructs may require mechanical reinforcement to withstand physiological weight-bearing forces. Additionally, the reliance on a single chondrocyte source rather than a co-culture system limits the recapitulation of complex signaling at the osteochondral interface. Finally, as this study was conducted under static in vitro conditions without quantitative interfacial shear testing, future work must address in vivo integration and durability under dynamic loading.

Conclusion

In this study, we developed a zone-specific, multilayer hydrogel construct inspired by the biochemical and biomechanical gradients of native articular cartilage. Individual hydrogel layers were systematically optimized in terms of methacrylation degree and PEGDMA content to replicate the structural and functional attributes of the superficial, middle, and deep cartilage zones.

Comprehensive physicochemical characterizations confirmed that each hydrogel formulation exhibited distinct and tunable swelling behavior, degradation kinetics, and porous microarchitecture. PEGDMA incorporation modulated hydration in a material-dependent manner, reducing swelling in CSMA-based hydrogels while enhancing it in GelMA systems, highlighting the role of polymer-crosslinker interactions in regulating network behavior.

SEM analysis further supports these material-specific behaviors. GelMA-based scaffolds exhibited larger, more interconnected pores (50–200 μm), which are advantageous for nutrient diffusion and chondrocyte infiltration. This is likely due to the looser packing and flexible nature of the GelMA-PEGDMA network, which promotes the formation of well-defined, open porous architectures during polymerization. In contrast, CSMA hydrogels displayed more variable and denser porosity, where pore morphology was closely governed by the degree of methacrylation and crosslinking density. The stiffer polysaccharide chains and high functional group density in CSMA promote a more compact and brittle network upon PEGDMA addition, leading to smaller pore sizes and thinner walls. These findings underscore how base polymer chemistry, when coupled with crosslinker concentration, can be strategically leveraged to tune both hydration behavior and microarchitecture for zone-specific scaffold design in cartilage tissue engineering.

Mechanical testing confirmed a progressive increase in compressive modulus from superficial to deep layers (30–268 kPa), recapitulating the native cartilage gradient. Consistently, enzymatic degradation assays revealed that PEGDMA-modified hydrogels, particularly hydrogels with highly methacrylated GelMA-PEGDMA formulations, exhibited markedly reduced mass loss, reflecting the stabilizing effect of increased crosslinking density. These results collectively underscore the role of PEGDMA and methacrylation degree in enhancing both mechanical robustness and degradation resistance, thereby improving scaffold durability under physiologically relevant conditions.

Biological evaluations corroborated the functional advantages of this structural tuning. All hydrogel layers supported high chondrocyte viability and zone-appropriate expression profiles. Gene expression analysis of individually cultured chondrocytes within the zone-specific hydrogel formulations revealed distinct transcriptional profiles consistent with their respective anatomical mimics. Elevated COL2A1 and ACAN expression was observed in middle and deep zone constructs, reflecting enhanced chondrogenic activity, while COL10A1 upregulation in the nHA-enriched deep layer indicated early hypertrophic differentiation, a hallmark of calcified cartilage. These findings were further supported by immunofluorescence staining for collagen type II, which confirmed sustained matrix production across all groups. Together, these results affirm the biofunctional fidelity of the designed hydrogel compositions and underscore their potential to support zone-appropriate cellular phenotypes and extracellular matrix deposition critical for osteochondral regeneration.

These results collectively highlight the synergistic benefits of chemical and architectural tuning in engineering scaffolds that recapitulate the depth-dependent structural, mechanical, and biological complexity of native cartilage. The highly hydrated and porous superficial layer facilitates early cell infiltration, nutrient exchange, and tissue integration, while the denser and stiffer deep zone mimics the load-bearing mineralized cartilage-bone interface. Although the multilayered configuration was evaluated as a model system, its rational design and demonstrated functionality position it as a promising candidate for future translational studies. Future work will incorporate co-culture systems and fluorescent partition-tracking methods to evaluate interlayer synergy, cell migration patterns, and osteochondral interface integration. Ongoing efforts will focus on validating this construct in large animal models to assess its efficacy in osteochondral repair under load-bearing in vivo conditions.

Data availability

The datasets analyzed during the current study are available from the corresponding author on reasonable request.

Received: 5 September 2025; Accepted: 17 December 2025
Published online: 24 December 2025

References

1. Zurriaga Carda, J. et al. Articular cartilage regeneration with a microgel as a support biomaterial. A rabbit knee model. *Biomaterials Adv.* **168**, 214125 (2025).
2. Pueyo Moliner, A. et al. Restoring articular cartilage: insights from structure, composition and development. *Nat. Rev. Rheumatol.* **21** (5), 291–308 (2025).
3. Zhou, J. et al. An effective approach to cartilage regeneration using antler stem cell-conditioned medium. *Sci. Rep.* **15** (1), 27971 (2025).

4. Kalairaj, M. S. et al. Intra-articular injectable biomaterials for cartilage repair and regeneration. *Adv. Healthc. Mater.* **13** (17), 2303794 (2024).
5. Li, H. et al. Cartilage lacuna-biomimetic hydrogel microspheres endowed with integrated biological signal boost endogenous articular cartilage regeneration. *Bioactive Mater.* **41**, 61–82 (2024).
6. Li, C. S. et al. Ultramodern natural and synthetic polymer hydrogel scaffolds for articular cartilage repair and regeneration. *Biomed. Eng. Online*. **24** (1), 1–26 (2025).
7. Yang, Y. et al. Developmental dynamics mimicking inversely engineered pericellular matrix for articular cartilage regeneration. *Biomaterials* **317**, 123066 (2025).
8. Wang, C. et al. Injectable tissue-engineered human cartilage matrix composite fibrin glue for regeneration of articular cartilage defects. *Biomaterials Adv.* **167**, 214095 (2025).
9. Bordbar, S. et al. Cartilage tissue engineering using decellularized biomatrix hydrogel containing TGF-β-loaded alginate microspheres in mechanically loaded bioreactor. *Sci. Rep.* **14** (1), 11991 (2024).
10. Hashemi-Afzal, F. et al. Advancements in hydrogel design for articular cartilage regeneration: A comprehensive review. *Bioactive Mater.* **43**, 1–31 (2025).
11. Kang, Y., Guan, Y. & Li, S. Innovative hydrogel solutions for articular cartilage regeneration: a comprehensive review. *Int. J. Surg.* **110** (12), 7984–8001 (2024).
12. Zhang, H. et al. Monophasic hyaluronic acid-silica hybrid hydrogels for articular cartilage applications. *Biomaterials Adv.* **167**, 214089 (2025).
13. Lin, L. et al. Alkaline phosphatase-instructed self-assembling supramolecular glucosamine hydrogel for osteoarthritis treatment. *Biomaterials Adv.* **178**, 214451 (2026).
14. He, S. et al. Construction of a dual-component hydrogel matrix for 3D biomimetic skin based on photo-crosslinked chondroitin sulfate/collagen. *Int. J. Biol. Macromol.* **254**, 127940 (2024).
15. Xue, H. et al. Polydopamine-coated chondroitin sulfate methacryloyl multifunctional microspheres for wound treatment. *Int. J. Biol. Macromol.* **280**, 136087 (2024).
16. Murphy, C. A., Serafin, A. & Collins, M. N. Development of 3D printable gelatin methacryloyl/chondroitin sulfate/hyaluronic acid hydrogels as implantable scaffolds. *Polymers*, **16**(14), 1958 (2024).
17. Mistretta, K. S. et al. Local sustained Dinutuximab delivery and release from methacrylated chondroitin sulfate. *J. Biomedical Mater. Res. Part. A*. **113** (1), e37803 (2025).
18. Xu, W. et al. Engineered Biomechanical microenvironment of articular chondrocytes based on heterogeneous GelMA hydrogel composites and dynamic mechanical compression. *Biomaterials Adv.* **153**, 213567 (2023).
19. Klara, J. et al. Photocrosslinked gelatin/chondroitin sulfate/chitosan-based composites with tunable multifunctionality for bone tissue regeneration. *Int. J. Biol. Macromol.* **271**, 132675 (2024).
20. Chen, R. et al. Facile synthesis of mechanically robust and injectable tetra-polyethylene glycol/methacrylate Chitosan double-network hydrogel cartilage repair. *Polym. Test.* **133**, 108410 (2024).
21. Golebiowska, A. A. et al. Engineered osteochondral scaffolds with bioactive cartilage zone for enhanced articular cartilage regeneration. *Ann. Biomed. Eng.* **53** (3), 597–611 (2025).
22. Hu, J. et al. Zonal characteristics of collagen ultrastructure and responses to mechanical loading in articular cartilage. *Acta Biomater.* **195**, 104–116 (2025).
23. Taghizadeh, S. et al. Magnetic hydrogel applications in articular cartilage tissue engineering. *J. Biomedical Mater. Res. Part. A*. **112** (2), 260–275 (2024).
24. Wu, Y. et al. Improved articular cartilage repair with stratified zonal chondrocyte implantation. *Am. J. Sports Med.* **53** (9), 2094–2106 (2024).
25. Li, G. et al. Key roles of the superficial zone in articular cartilage physiology, pathology, and regeneration. *Chin. Med. J.* **138** (12), 1399–1410 (2025).
26. Cao, F., Li, P. & Guo, L. Bibliometric and visualization analysis of superficial zone of articular cartilage from 2000 to 2024. *Osteoarthr. Cartil.* **33** (6), 777 (2025).
27. Ye, T. et al. Lysosomal destabilization: a missing link between pathological calcification and osteoarthritis. *Bioactive Mater.* **34**, 37–50 (2024).
28. Wu, X. et al. A 3D printed multilayer biomimetic scaffold with a gradient-oriented structure for articular cartilage repair. *J. Mater. Chem. B.* **13**, 7728–7743 (2025).
29. Silva, B. et al. Toward integrative Biomechanical models of osteochondral tissues: A multilayered perspective. *Bioengineering* **12** (6), 649 (2025).
30. Nikhil, A. et al. Multilayered cryogel enriched with exosomes regenerates and maintains cartilage architecture and phenotype in goat osteochondral injuries. *ACS Appl. Mater. Interfaces*. **16** (47), 64505–64521 (2024).
31. Moradian, A. et al. Photo- and thermal-crosslinked GelMA/chitosan hydrogels: A novel approach to enhanced mechanical and biological properties. *Carbohydr. Polym. Technol. Appl.* **10**, 100834 (2025).
32. Raikov, B. et al. Methods for determining the molecular composition of knee joint structures in osteoarthritis: collagen, proteoglycans and water content: a systematic review. *Collagen Leather*. **6** (1), 30 (2024).
33. Çelik, E. et al. Calcified and mechanically debilitated three-dimensional hydrogel environment induces hypertrophic trend in chondrocytes. *J. Bioactive Compatible Polym.* **31** (5), 498–512 (2016).
34. Peters, J. R. et al. Tissue growth as a mechanism for collagen fiber alignment in articular cartilage. *Sci. Rep.* **14** (1), 31121 (2024).
35. Singh, J. et al. Biomimetic double network hydrogels of chondroitin sulfate and synthetic polypeptides for cartilage tissue engineering. *Biomaterials Sci.* **13**, 4211–4231 (2025).
36. Park, S. et al. Polydeoxynucleotide-loaded visible light photo-crosslinked gelatin methacrylate hydrogel: approach to accelerating cartilage regeneration. *Gels* **11** (1), 42 (2025).
37. Yu, J. et al. Versatile chondroitin sulfate-based nanoplatform for chemo-photodynamic therapy against triple-negative breast cancer. *Int. J. Biol. Macromol.* **265**, 130709 (2024).
38. Fowler, M. et al. Guiding vascular infiltration through architected GelMA/PEGDA hydrogels: an in vivo study of channel diameter, length, and complexity. *Biomaterials Sci.* **13** (11), 2951–2960 (2025).
39. Golini, C. et al. Depth-wise multiparametric assessment of articular cartilage layers with single-sided NMR. *NMR Biomed.* **38** (1), e5287 (2025).
40. Beck, E. C. et al. Approaching the compressive modulus of articular cartilage with a decellularized cartilage-based hydrogel. *Acta Biomater.* **38**, 94–105 (2016).
41. Gorroñogoitia, I. et al. The effect of Alginate/Hyaluronic acid proportion on Semi-Interpenetrating hydrogel properties for articular cartilage tissue engineering. *Polymers* **17** (4), 528 (2025).
42. Liang, J. et al. Hybrid hydrogels based on Methacrylate-Functionalized gelatin (GelMA) and synthetic polymers. *Biomedical Mater. Devices*. **1** (1), 191–201 (2023).
43. Rodrigues, L. C. et al. 3D tubular constructs based on natural polysaccharides and Recombinant polypeptide synergistic blends as potential candidates for blood vessel solutions. *Int. J. Biol. Macromol.* **310**, 143084 (2025).
44. Dabaja, R. et al. Spatially distributed and interconnected porous architectures for dental implants. *Int. J. Implant Dentistry*. **11** (1), 30 (2025).

45. Salehi, M. et al. Achieving biomimetic porosity and strength of bone in magnesium scaffolds through binder jet additive manufacturing. *Biomaterials Adv.* **166**, 214059 (2025).
46. Mukasheva, F. et al. Optimizing scaffold pore size for tissue engineering: Insights across various tissue types. *Front. Bioeng. Biotechnol.* **12**, 1444986 (2024).
47. Chonanant, C. et al. Biocomposite scaffolds based on Chitosan extraction from shrimp shell waste for cartilage tissue engineering application. *ACS Omega.* **9** (38), 39419–39429 (2024).
48. Welsh, B. L. & Sikder, P. Advancements in cartilage tissue engineering: A focused review. *J. Biomedical Mater. Res. Part. B: Appl. Biomaterials.* **113** (1), e35520 (2025).
49. Gonella, S. et al. Fabrication and characterization of porous PEGDA hydrogels for articular cartilage regeneration. *Gels* **10** (7), 422 (2024).
50. Kurian, A. G. et al. Multifunctional GelMA platforms with nanomaterials for advanced tissue therapeutics. *Bioactive Mater.* **8**, 267–295 (2022).
51. Wang, H. et al. Comparing the effect of mechanical loading on deep and superficial cartilage using quantitative Ute mri. *J. Magn. Reson. Imaging.* **59** (6), 2048–2057 (2024).
52. Choi, H., Choi, W. S. & Jeong, J. O. A review of advanced hydrogel applications for tissue engineering and drug delivery systems as biomaterials. *Gels* **10** (11), 693 (2024).
53. Mow, V. C., Ratcliffe, A. & Robin Poole, A. Cartilage and diarthrodial joints as paradigms for hierarchical materials and structures. *Biomaterials* **13** (2), 67–97 (1992).
54. Dong, D. L. & Jin, G. Z. Targeting chondrocyte hypertrophy as strategies for the treatment of osteoarthritis. *Bioengineering* **12** (1), 77 (2025).
55. Pan, X. et al. Biomimetic vascular scaffolds via hybrid 3D printing-phase separation for vascularized cardiac tissue with enhanced perfusion and maturation. *Biomaterials Sci.* **13** (17), 4803–4815 (2025).
56. Cai, H. et al. Vascular network-inspired diffusible scaffolds for engineering functional midbrain organoids. *Cell. Stem Cell.* **32** (5), 824–837 (2025). e5.
57. Hudson, A. R. et al. Enhancing viability in static and perfused 3D tissue constructs using sacrificial gelatin microparticles. *ACS Biomaterials Sci. Eng.* **11** (5), 2888–2897 (2025).
58. Owida, H. A. et al. Induction of zonal-specific cellular morphology and matrix synthesis for biomimetic cartilage regeneration using hybrid scaffolds. *J. Royal Soc. Interface.* **15** (143), 20180310 (2018).
59. Ghadirian, S., Shariati, L. & Karbasi, S. Evaluation of the effects of cartilage decellularized ECM in optimizing PHB-chitosan-HNT/chitosan-ECM core-shell electrospun scaffold: physicochemical and biological properties. *Biomaterials Adv.* **172**, 214249 (2025).
60. Amanatullah, D. F., Yamane, S. & Reddi, A. H. Distinct patterns of gene expression in the superficial, middle and deep zones of bovine articular cartilage. *J. Tissue Eng. Regen. Med.* **8** (7), 505–514 (2014).
61. Liu, Y. et al. Bioprinted biomimetic hydrogel matrices guiding stem cell aggregates for enhanced chondrogenesis and cartilage regeneration. *J. Mater. Chem. B.* **12** (22), 5360–5376 (2024).
62. Zheng, K. et al. Co-culture pellet of human wharton's jelly mesenchymal stem cells and rat costal chondrocytes as a candidate for articular cartilage regeneration: in vitro and in vivo study. *Stem Cell Res. Ther.* **13** (1), 386 (2022).
63. Zhang, L. et al. Multileveled hierarchical hydrogel with continuous biophysical and biochemical gradients for enhanced repair of full-thickness osteochondral defect. *Adv. Mater.* **35** (19), 2209565 (2023).
64. Wu, J. et al. Regional-specific meniscal extracellular matrix hydrogels and their effects on cell-matrix interactions of fibrochondrocytes. *Biomed. Mater.* **17** (1), 014105 (2021).
65. Decarli, M. C. et al. Bioprinting of stem cell spheroids followed by post-printing chondrogenic differentiation for cartilage tissue engineering. *Adv. Healthc. Mater.* **12** (19), 2203021 (2023).

Author contributions

Ekin Çelik: Writing-original draft, Methodology, Visualization, Investigation, Data curation, Formal analysis, Conceptualization. Cem Bayram: Supervision, Writing, Methodology, Data curation, Visualization, Investigation. Emir Baki Denkbaş: Resources, Project administration, Methodology, Supervision. All authors reviewed and edited the manuscript.

Funding

The present study was carried out without external project funding.

Declarations

Competing interests

The authors declare no competing interests.

Additional information

Supplementary Information The online version contains supplementary material available at https://doi.org/10.1038/s41598-025-33222-0.

Correspondence and requests for materials should be addressed to E.Ç.